Available online at www.sciencedirect.com
SCIENCE DIRECT
Atmospheric Environment 40 (2006) 3969–3982
ATMOSPHERIC ENVIRONMENT
www.elsevier.com/locate/atmosenv

Influence of topography and land use on pollutants dispersion in the Atlantic coast of Iberian Peninsula

A.C. Carvalho[a,*], A. Carvalho[a], I. Gelpi[b], M. Barreiro[b], C. Borrego[a], A.I. Miranda[a], V. Pérez-Muñuzuri[b]

[a]*Department of Environment and Planning, University of Aveiro, 3810-193 Aveiro, Portugal*
[b]*Grupo de Física No Lineal, Unidad de Observación y Predicción Meteorológica, Facultad de Físicas, Universidad de Santiago de Compostela, Spain*

Received 14 September 2005; received in revised form 1 February 2006; accepted 15 February 2006

Abstract

The west coast of Iberian Peninsula, surrounded by the Atlantic Ocean, is characterised by complex topography and specific synoptical situations that imply mesoscale circulations development. The main purpose of this work is to analyse how mesoscale circulations induced by topography and/or land use control pollutants dispersion in a coastal region. A numerical system combining the MM5 meteorological model and the air-quality model MARS was applied to the north western part of Portugal mainland. This system of models simulated the dispersion of pollutants in the atmosphere during two consecutive summer days under the influence of a thermal low-pressure system located over the Iberian Peninsula. To analyse the photo-chemical production inside the domain of interest an interface between MM5 and the photo-chemical model MARS was built up, constituting the first attempt to integrate these two models. MM5 and MARS sensitivity tests were performed for different conditions starting with null topography and homogeneous land use. The achieved results revealed that the mesoscale circulations that are developed in the west coast of Iberian Peninsula are mainly related to topographic effects instead of land–sea thermal-induced ones. Topography represented the main driving force mechanism on air pollutants injection in higher tropospheric levels.

Keywords: Physiographical aspects; Thermal-induced circulations; Ozone patterns

1. Introduction

Topography and land use play an important role on synoptical patterns changes through mesoscale systems development, namely sea/land breezes, heat islands, and anabatic/katabatic winds (Stull, 1991). In Portugal, coastal mesoscale meteorology is strongly connected with ozone production and transport as shown in previous works by Borrego et al. (2000), Barros et al. (2003), and Monteiro et al. (2005). Monteiro (2003) has applied a hydrostatic photo-chemical model system in order to evaluate land-use change on surface-ozone patterns pointing out an increase of ozone concentration levels when water is absent. Studies on atmospheric circulations over the Iberian Peninsula have shown particularities concerning summer dynamics (Millan

*Corresponding author. Fax: +351 234 429290.
E-mail address: anacarv@dao.ua.pt (A.C. Carvalho).

1352-2310/$ - see front matter © 2006 Elsevier Ltd. All rights reserved.
doi:10.1016/j.atmosenv.2006.02.014

et al., 1992). Frequently, there is the development of a low thermal pressure region in the centre of the Peninsula, which allows mesoscale processes enhancement such as land–sea breezes (Martín et al., 2001). In the presence of complex terrain near coastlines, these mesoscale phenomena may be combined with anabatic/katabatic winds creating recirculations along shore. Millán et al. (1997), Salvador et al. (1997), and Choi (2003) have addressed this issue in east Iberian Peninsula and in a Korean coastal region. This type of circulations encourages photo-chemical production of air pollutants leading to smog episodes, which can cause health problems to the population and environmental degradation (Barna and Lamb, 2000). According to Millán et al. (1996) high ozone concentrations can be recorded in some strata in the mid-troposphere, all over the Iberian Peninsula and the western Mediterranean sea, which have been associated to the combined effect of the Iberian thermal low in summer and the topographic injection produced by some mountain ranges. Those authors also concluded that the vertical distribution of the low-mid tropospheric ozone in Spain is governed in spring and in summer by mesoscale systems, which determine its long transport. Then, the knowledge and characterisation of mesoscale atmospheric flow patterns, as well as, the description, by mathematical models, of dispersion and transformation mechanisms of photo-oxidants are fundamental. The present work investigates how photo-oxidant pollutants formation and dispersion is conditioned by topography and land use in the Atlantic coast of the Iberian Peninsula. This paper is organised as follows: Section 2 describes the applied numerical models. The methodology is given in Section 3, and model results are examined in Section 4. Section 5 provides a brief summary of the work.

2. The applied numerical models: MM5/MARS

The chosen meteorological model for this study is the nonhydrostatic Pennsylvania State University/National Center for Atmospheric Research Mesoscale Meteorology Model MM5 (Dudhia, 1993; Grell et al., 1994). MM5 is a powerful meteorological model that contains comprehensive descriptions of atmospheric motions; pressure, moisture, and temperature fields; momentum, moisture, and heat fluxes; turbulence, cloud formation, precipitation, and atmospheric radiative characteristics. The MM5 is a nested-grid primitive-equation model that uses a terrain-following sigma (nondimensionalised pressure) vertical coordinate. The MARS model numerically simulates photo-oxidants formation considering the chemical transformation process of pollutants together with its transport in the atmospheric boundary layer (Moussiopoulos et al., 1995). This model is directed towards the photo-oxidants simulation, from which ozone (O_3) is the major component. KOREM and RADM2 can be used on MARS as chemical mechanisms. The first one, which has been chosen in this work, includes 39 chemical reactions with 20 reactive pollutants. Both chemical mechanisms were already tested and evaluated for this study region. Although of lesser complexity, KOREM revealed good results (Miranda et al., 2002; Ferreira et al., 2003). The model solves the parabolic differential concentration transport equation system in terrain-following co-ordinates, in a fully vectorised way, with the meteorological variables calculated by MM5, e.g., the mass conservation equations are driven by the momentum equation. In addition to the meteorological fields, MARS model needs daily variable chemical species emissions as inputs. These are calculated based on proper approaches depending on the emissions of air pollutants emitted by anthropogenic and biogenic sources. These two models have been applied worldwide by a variety of entities. MM5 is a wide spread community model with strong user support, that is being tested all over the world (Barna and Lamb, 2000; Seaman, 2000; Elbern and Schmidt, 2001; Sistla et al., 2000). In Iberian Peninsula several institutions are applying MM5 as a real-time weather forecasting model (http://meteo.usc.es) and also as a research tool (http://redibericamm5.uib.es). MARS is also a well-tested model over several Iberian urban airsheds (Baldasano et al., 1993; San José et al., 1997; Borrego et al., 1998).

3. Methodology

The system of models (MM5 and MARS) is used to simulate a selected O_3 episode observed in the Portuguese coastal region under a thermal low-pressure system. The simulate meteorological fields and concentrations of photo-oxidant are then compared with available observations. The mesoscale circulations that are developed during the period under study are also analysed.

3.1. MM5 model application

MM5 model simulates 54 h, starting at 18 h00 UTC 14 June 2000 till 17 June at 00 h, to allow for numerical spin up, for the first 6 h simulation. The numerical model MARS is applied from 15 June, 00 h, to 17 June, 00 h, 2000. During 15 June high pressure becomes established over Biscay Gulf for some days stabilising the atmosphere all over the Iberian Peninsula. Moreover, the advection is from SE, leading to very high surface temperatures, competing with the stable atmosphere. In this way a low pressure centre of thermal origin appears over north Africa, extending its influence to the SE of Iberian Peninsula. On 16 June, high pressure continues stationary over Biscay Gulf, with a ridge area dominating west part of Iberian Peninsula. The low-pressure system of thermal origin is located over the SE Iberian Peninsula. (http://www.wetterzentrale.de/topkarten/fsavneur.html). Using MM5 capability of doing multiple nestings, the meteorological model is applied for two nests: (i) a large domain covering the Iberian Peninsula (45 km resolution), (ii) a first nest covering the Atlantic Coast of Iberian Peninsula (15 km resolution), (iii) and a second nest over the north part of Portugal (5 km resolution) (Fig. 1). Several attempts are tried in order to investigate the adequate number of sigma (σ) levels and physics parameterisations for the improvement of the thermal low-pressure system simulation. It is concluded (not shown in this paper) that the default σ levels specification (23, with the first layer height at 36 m) is not sufficient to resolve the meteorological phenomena under study. Sensitivity studies were made with 35 and 40 σ levels, which results considerable improvements on simulated values, mainly due to vertical resolution increase near ground. Considering these achievements and computational constraints, new 23 σ levels are defined in order to optimise the simulation through the increase of the vertical resolution near the ground. MM5 simulations are initialised with the global reanalysis data from the National Center for Environmental Prediction and from the National Center for Atmospheric Research (NCEP/NCAR), producing outputs in nested 45, 15, and 5 km grids. The grid sizes are 27×31, 31×43, and 40×40 grid points, respectively. All modelling domains have the same vertical structure with 23 unequally spaced σ levels, with a maximum resolution near ground of 8 m. The 5 km grid is governed by the Reisner graupel microphysics moisture scheme, Kain–Fritsch cumulus parameterisation, and the ETA boundary layer scheme.

The sensitivity analysis on vertical O_3 concentration fields is carried out using the factor analysis developed by Stein and Alpert (1993). According to these authors 2^n simulations are required to correctly evaluate the contribution and the interaction between the n factors. The inner domain (40×40 grid cells with 5×5 km resolution) topography and land use are modified in order to evaluate the influence of these two important features on the local to regional flow patterns. In this study a set of four simulations are performed (Table 1). The modified characteristics include constant height as flat terrain at 0 m and constant

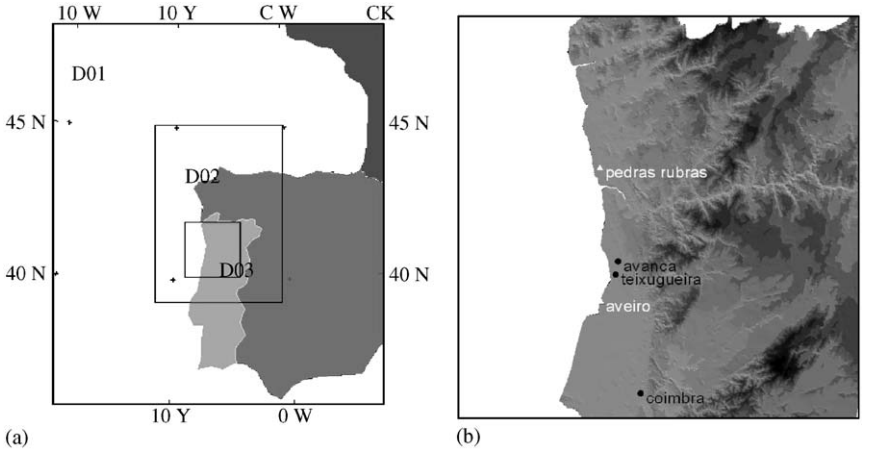

Fig. 1. (a) MM5 simulation domains, and (b) meteorological (in white) and air-quality (in black) stations location over the innermost domain.

Table 1
Sensitivity analysis options

	Land use	Topography
Simulation 1	USGS	USGS
Simulation 2	USGS	Null
Simulation 3	Constant	USGS
Simulation 4	Constant	Null

land use defined as mixed shrub and grassland (code 9 from the United States Geological Survey-USGS database).

3.2. Interface between MM5 and MARS

In order to analyse the photo-chemical production over the innermost domain, an interface between MM5 and the photo-chemical model MARS is developed. With this interface all the needed meteorological parameters to calculate photo-chemical air pollutants advection, production, and removal are fed into the photo-chemical model with the necessary time-step resolution. The meteorological variables are interpolated from the MM5 Arakawa B horizontal grid to the MARS C grid (further details on Arakawa grids in Alder et al. (1977)). 2D fields of Monin–Obukhov length and non dimensional roughness, $\ln(Z/Z_0)$, are also included.

3.3. MARS model application

The MARS model is applied to the innermost domain ($200 \times 200\,km^2$ with $5 \times 5\,km^2$ resolution) with MM5 outputs and the calculated pollutant emissions grid. Anthropogenic emissions are calculated applying a disaggregation technique from the national level to the municipal and then to the sub-municipal level. The CORINAIR 95 National Inventory is used to estimate emission data with required spatial and temporal resolution based on statistical indicators. As a first step, national emission data are disaggregated to the municipal level using fuel consumption. Then, the data are processed jointly with population statistics in order to obtain sub-municipal resolution.

The pollutants emissions are disaggregated for the different chemical species considered in the KOREM mechanism, through the application of a pre-processor that considers the following assumptions:

- For industrial and commercial sources, an average volatile organic compounds (VOCs) profile is applied, based on the VOCs profile for coal, fuel oil and natural gas combustion (Schneider, 1994); nitrogen oxides (NO_x) is considered as 90% nitrogen monoxide (NO) and 10% nitrogen dioxide (NO_2) (EC, 1994).
- For road traffic, the VOCs profile is based on the typical profiles for gasoline and fuel combustion (Costa, 1995); NO_x is defined as 83% of NO and 17% of NO_2.
- For point sources, VOCs profile is established according to the production process; for thermal power plants this is based on the used fuel (Schneider, 1994; EC, 1994).

The estimated point sources emissions are allocated in the vertical direction of the 3D mesh considering the stack height and the plume rise of the exhaust gases. The area sources are considered at the ground level (first level of the model). The initial and boundary conditions are based on the background concentrations for the chemical species considered within MARS model (Moussiopoulos et al., 1995; Barros, 1999). Biogenic emissions are not considered in this work.

4. Results and discussion

As referred on methodology, four MM5 simulations are performed for the innermost domain. Simulation 1 considers USGS characteristics of topography and land use. This means that all the terrain available databases are interpolated from the 30 s resolution (around 1 km) global coverage as well as the land use database, which groups land use in 25 categories. Simulation 2 is performed for flat terrain (0 m) and USGS land use and Simulation 3 for USGS topography and constant mixed shrub and grassland instead of water code, avoiding abrupt changes between land use over coastal regions and the area of the domain previously covered with the Atlantic Ocean. Simulation 4 considers flat terrain and constant land use (mixed shrub and grassland) for the overall simulation domain. To better assess MM5/MARS application to the inner domain, the outputs analysis is subdivided into two parts: meteorology and air-quality analysis. Concerning MM5 model performance on coastal meteorological phenomena, two stations are selected for its assessment, Aveiro and Pedras Rubras (Fig. 1). The air-quality stations selected for MARS evaluation are Teixugueira, Estarreja and Coimbra, representing a rural, an industrial and

an urban one, respectively (Fig. 1). The models skills are evaluated through statistical analysis procedure and direct comparison between the hourly averaged estimated and measured data. The statistical analysis applied is based on Keyser and Anthes (1977) and Pielke (2002). Consequently, if ϕ_i and $\phi_{i,\mathrm{obs}}$ are individual modelled and observed data in the same grid cell, respectively, ϕ_0 and $\phi_{0,\mathrm{obs}}$ the average of ϕ_i and $\phi_{i,\mathrm{obs}}$ for some sequence in study, and N the number of observations, then

$$E = \left\{ \frac{\sum_{i=1}^{N} \left(\phi_i - \phi_{i,\mathrm{obs}}\right)^2}{N} \right\}^{1/2},$$

$$E_{\mathrm{UB}} = \left\{ \frac{\sum_{i=1}^{N} \left[\left(\phi_i - \phi_0\right) - \left(\phi_{i,\mathrm{obs}} - \phi_{0,\mathrm{obs}}\right)\right]^2}{N} \right\}^{1/2},$$

$$S = \left\{ \frac{\sum_{i=1}^{N} \left(\phi_i - \phi_0\right)^2}{N} \right\}^{1/2},$$

$$S_{\mathrm{obs}} = \left\{ \frac{\sum_{i=1}^{N} \left(\phi_{i,\mathrm{obs}} - \phi_{0,\mathrm{obs}}\right)^2}{N} \right\}^{1/2}.$$

The parameter E represents the root mean square error (rmse), E_{UB} the rmse after the removal of a constant bias (that can be related to inaccuracy in specifications of the initial and boundary conditions) and S and S_{obs} the standard deviation of the modelled and observed data, respectively. The model skill is good when $S \approx S_{\mathrm{obs}}$, $E < S_{\mathrm{obs}}$ and $E_{\mathrm{UB}} < S_{\mathrm{obs}}$.

4.1. MM5 model evaluation

For the present study, meteorological measurements are available at two locations over the study region, Pedras Rubras and Aveiro. MM5 results are compared against the meteorological data acquired at the referred stations. Table 2 presents the statistical analysis results for each meteorological variable for Simulation 1 over the innermost domain.

The statistical parameters reveal that MM5 presents a good skill for temperature but wind speed and direction are roughly represented in the evaluated stations. This can be related to the boundary conditions coarse resolution, i.e., spatial resolution of the initial meteorological fields may be insufficient to reproduce the thermal-low conditions over the Iberian Peninsula. Another reason may be related to the use of skin-temperature fields instead of sea-surface temperature as surface boundary conditions driver. The temporal evolution of the meteorological parameters, measured and estimated, at each station allows to better understand the obtained skills. The model poorly represents wind velocity, particularly during the night overestimating the simulated values. Wind direction is well simulated by MM5 at Pedras Rubras station although, during the afternoon in both days, there is a time lag between measured and modelled values. At Aveiro station the simulated wind direction presents differences relative to the measured values, and this can be related to the meteorological station location near the Aveiro lagoon, suffering influences not well simulated by the model due to its coarse resolution. Notwithstanding these identified simulation weaknesses, the MM5 model reasonably simulates the local atmospheric conditions that characterise the considered period although it underestimates temperature and wind velocity at the first hours of simulation in Pedras Rubras and overestimates at Aveiro. Also, the MM5 simulates the sea breeze front entrance which is detected at noon temperature values.

4.2. MARS model evaluation

Concerning air-quality data availability, O_3 measurements are accessible at three different locations

Table 2
Statistical analysis of meteorological variables estimated by MM5 model

	S/S_{obs}		E/S_{obs}		$E_{\mathrm{UB}}/S_{\mathrm{obs}}$	
	Aveiro	Pedras Rubras	Aveiro	Pedras Rubras	Aveiro	Pedras Rubras
Temperature	0.98	1.02	0.65	0.69	0.54	0.68
Wind direction	0.87	0.99	1.17	1.10	1.05	1.08
Wind velocity	0.59	0.52	1.45	1.03	1.06	1.13

over the study region: Coimbra, Avanca and Teixugueira, these two stations belongs to the Eslarreja municipality (Fig. 1). Coimbra is an urban air-quality station, and for that reason, maximum O_3 concentrations are 86 and 88 $\mu g\,m^{-3}$, both occurring at noon of the 15 and 16 June, 2000 (Fig. 2a)). On the other hand, Teixugueira air-quality station (located near an industrial complex) and Avanca (considered a background measuring site) present the O_3 peak during the afternoon, around 17 h and 18 h UTC, over 160 $\mu g\,m^{-3}$ (Fig. 2b)). The occurrence time of these two peaks, on both days, indicates that the O_3 present in these locations may be due to plume production and advection from northern urban areas. Fig. 2 presents a direct comparison between modelled and measured O_3 concentrations at the three air-quality stations, Coimbra, Teixugueira and Avanca.

The MM5/MARS system shows the same pattern as the measured O_3 concentrations, although the peaks of O_3 are underestimated for Estarreja (the cell containing both Teixugueira and Avanca for the applied resolution of $5 \times 5\,km^2$). Over Coimbra the system of models tends to overestimate O_3 concentrations during the night (Fig. 2a)). Table 3 presents the statistical analysis of MARS model application.

According to Table 3, Coimbra station presents the worst quality indicators. This may be related to the local characteristics of this urban station, just beside a high-traffic road, where results are compared to an average simulated value from a $5 \times 5\,km^2$ grid cell. The low values obtained for the quality indicator S/S_{obs} points out that the system of models poorly simulates the natural variability of the measured O_3 data. The obtained E/S_{obs} and E_{UB}/S_{obs}, over Avanca and Teixugueira, reveals that the model produces acceptable results. Once that Teixugueira presents the best-data variability one can say that this station can be considered as a representative air-quality station for the defined modelling conditions. Based on the measured data over Teixugueira and Avanca (Fig. 2b)) it is possible to verify that the air-quality stations location is very important for validation studies at regional scale. Avanca presents O_3 decrease over night, which does not occur at Teixugueira.

4.3. Flow-patterns analysis

Although the main objective of this work is to investigate how sea and land breezes, associated with major topographic features near the coastline, may influence air quality over the region of interest, flow-patterns analysis at a regional scale is also addressed. In this sense, horizontal and vertical cross-sections are plotted for different meteorological variables, for the coarse and innermost domain. For MM5, coarse domain streamlines, at σ level corresponding to approximately 1500 m geopotential height, are analysed, in order to minimise

Table 3
Statistical analysis of O_3 concentrations estimated by MARS model

Air quality stations	Quality indicators		
	S/S_{obs}	E/S_{obs}	E_{UB}/S_{obs}
Avanca	0.49	0.59	0.59
Teixugueira	0.72	0.60	0.60
Coimbra	0.58	1.01	0.71

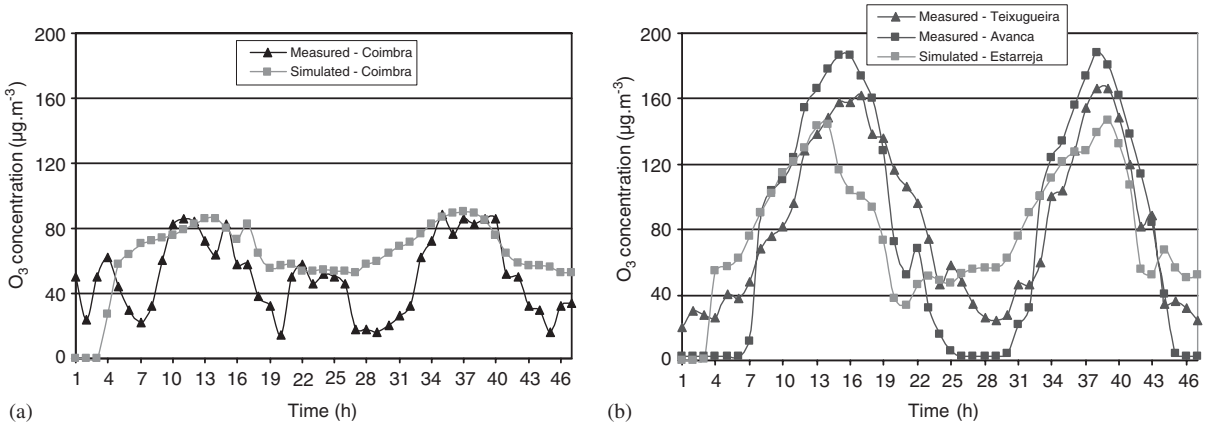

Fig. 2. O_3 concentration values, measured and simulated, at (a) Coimbra, and (b) Teixugueira and Avanca, located at Estarreja and Estarreja, for the simulated period (15 and 16 June 2000).

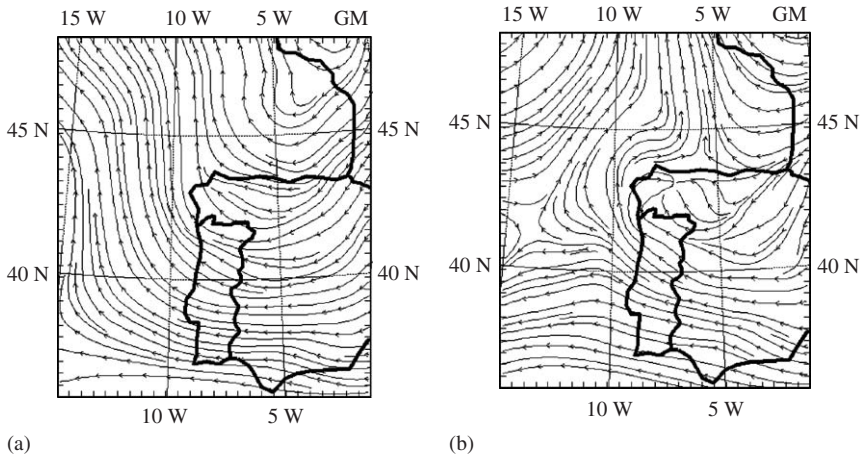

Fig. 3. MM5 coarse domain streamlines at 12 UTC for (a) 15 June and (b) 16 June 2000.

terrain height influence on flow patterns. Throughout the simulation period these streamlines come from the eastern part of the Iberian Peninsula directed to the Atlantic Ocean, which drift northward. At this level the atmospheric flow over Portugal is from east, showing greater intensities over the centre and southern part of the country (Fig. 3).

Hereafter, a short description of atmospheric vertical movement is made based on isentropic and wind velocity vertical component isotach analysis. Fig. 4 presents the vertical velocities ($cm\,s^{-1}$) and potential temperature (K) for both days in the MM5 coarse domain cross section at latitude 40.11 °N and longitude between 14.35 °W and 1.70 °W (over Estarreja). Dashed lines represent negative vertical velocities and solid lines positive ones.

Although isentropic analysis near the ground is compromised due to diabatic radiative heating/cooling processes, model results indicate greater static stability during 15 June (Fig. 4a)). During 15 June 2000 the isentropic slopes down from east to west. It is also observed that there are vertical compensating mechanisms producing cells of positive and negative isotachs. During the night, vertical movement is predominant subsiding over land. It is interesting to note the evolution of a nocturnal frontal system near shore, presenting positive vertical velocities over water and negative over the descending part of the mountain slope. This descending movement is pushed to the first terrain ridge (direction west to east) around noon in both days. This situation evolves to a series of close upwards and downwards cells over land. At 15 UTC the upward movements extends over 600 hPa, indicating a great penetration into the free atmosphere. At 18 UTC these upward movements reach their maximum extent at approximately 300 hPa. Hoinka and Castro (2003) described the Iberian thermal low (ITL) characteristics based on climatological datasets from 1979 to 1993. According to the authors, the vertical structure of the ITL has its peak intensity at 18 UTC reaching vertical velocity values of more than $3\,cm\,s^{-1}$. According to Fig. 4, at 18 UTC, vertical velocity presents values above $4\,cm\,s^{-1}$. The vertical potential-temperature structure presents a typical well-mixed layer, showing the influence of a strong terrain steep near the Atlantic coast. Contrarily to Hoinka and Castro (2003), the stable stratification above the coastal region is not detected. The isentropes present perturbations well above the 700 hPa induced by the vertical motions derived from the thermal low. In this analysis the relative shallowness of the thermal low, which develops over the Iberian Peninsula during summer, is not detected. It should be noticed that two completely different situations are being compared: climatological analysis against specific episodic situations. The described vertical and horizontal movements should strongly influence the photochemical pollutants formation and dispersion in the Atlantic coast of the Iberian Peninsula.

4.4. Topography and land use sensitivity analysis

As established in Section 3, the sensitivity analysis relative to topography and land use is just performed for the innermost domain. This analysis

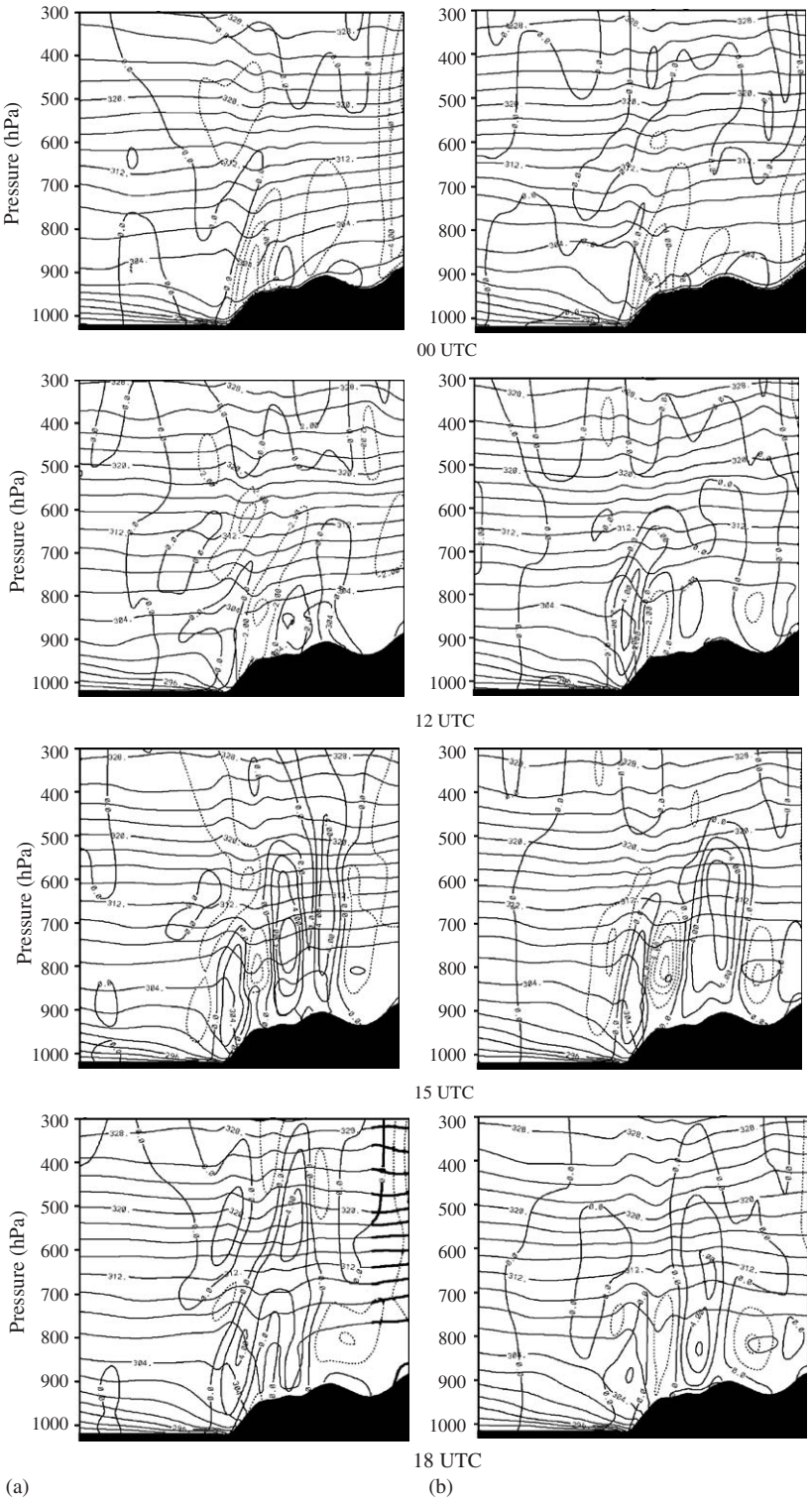

Fig. 4. Vertical velocity (cm s^{-1}) and potential temperature (K) over MM5 coarse domain cross-section at 00, 12, 15 and 18 UTC, for (a) 15 and (b) 16 June 2000.

is settled in order to better investigate the most important features that govern the pollutants dispersion in the study region. Fig. 5 presents vertical velocity and vertical potential temperature above the innermost domain for the different types of simulations, at 12 and 18 UTC for 15 June 2000. The presented cross-section is at latitude 40.11 °N, between 9.41 °W and 7.19 °W longitude (cross-section over Estarreja station). From Fig. 5a it is possible to verify that for simulation 1 (USGS land use and USGS topography) at 12 UTC the simulated domain presents a cell with positive vertical velocities above 32 cm s^{-1} just near the coast. The isentropics present deformations that are more pronounced below 800 hPa due to surface diabatic heating. Just side by side to the updrafts motions, subsidence cells can be detected with vertical velocities reaching the same magnitude as the updrafts. At 18 UTC the inland flow front is well developed and the updraft cell is located in the inner domain. Immediately, above the updraft motion there is a strong subsidence cell reaching velocities above 32 cm s^{-1}. In Simulation 2 (Fig. 5b) (USGS land use and null topography), at 12 UTC there is a convective cell above water with vertical updrafts above 16 cm s^{-1} and unchanged isentropics above 850 hPa. At 18 UTC there is a strong convective cell over water, reaching vertical velocities above 48 cm s^{-1} and isentropics reflect higher air mass expansion over land. In this case a pure sea breeze development is detected. Simulation 3 (Fig. 5c) (no water and USGS topography) at 12 UTC presents a much less intense convective cell in the west part of the domain, due to the water absence. Near the coast there is the development of a convective motion as it is detected in Simulation 1. At 18 UTC, this convective cell intensifies its vertical velocities (above 32 cm s^{-1}) due to temperature gradients that cause anabatic/katabatic winds, i.e., temperature gradients between surface slopes and environmental temperature at the same altitude. From this analysis it is possible to conclude that atmospheric thermal gradients derived from orographic effects are more important on inland-winds development.

Fig. 6 presents O_3 concentration vertical profiles for both days, at 12 and 18 UTC for Simulation 1.

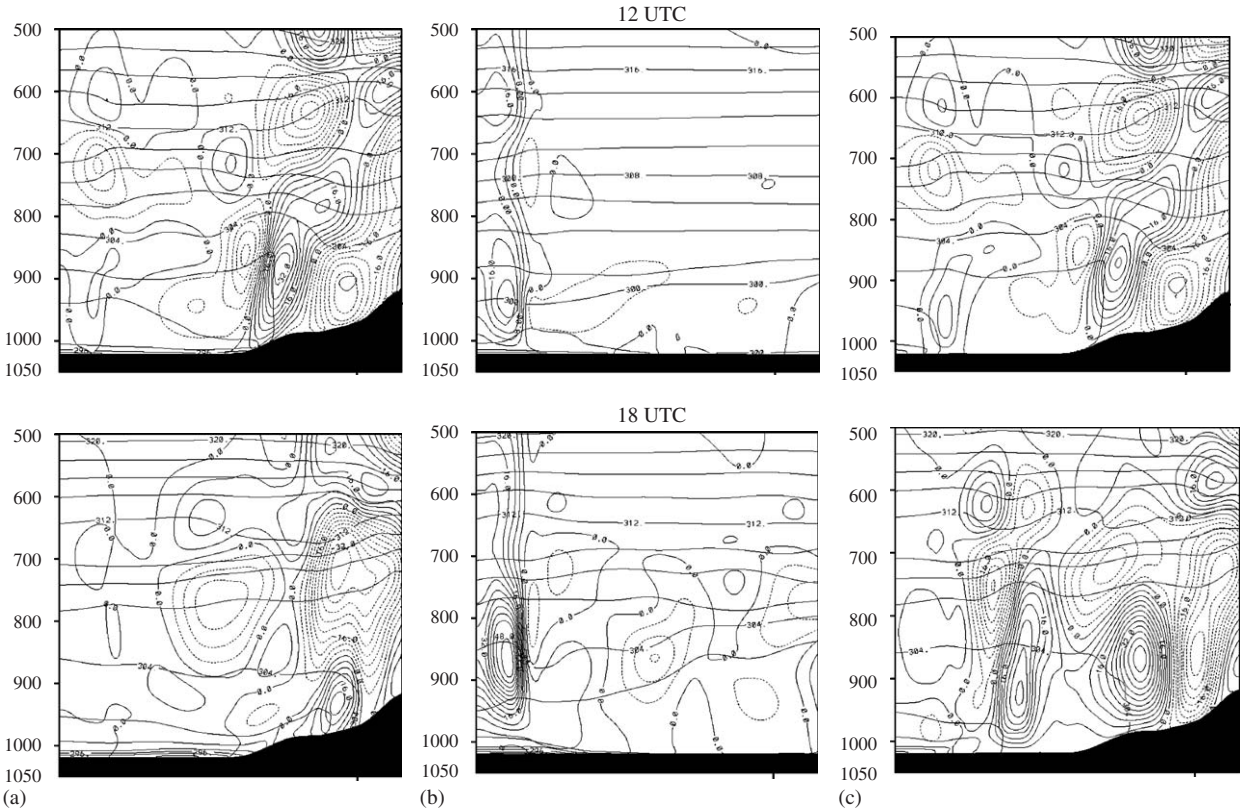

Fig. 5. Vertical velocities (cm s^{-1}) and vertical potential temperature (K) over the MM5 innermost domain cross-section for 15 June 2000, at 12 and 18 UTC, for (a) Simulation 1 (b) Simulation 2, and (c) Simulation 3.

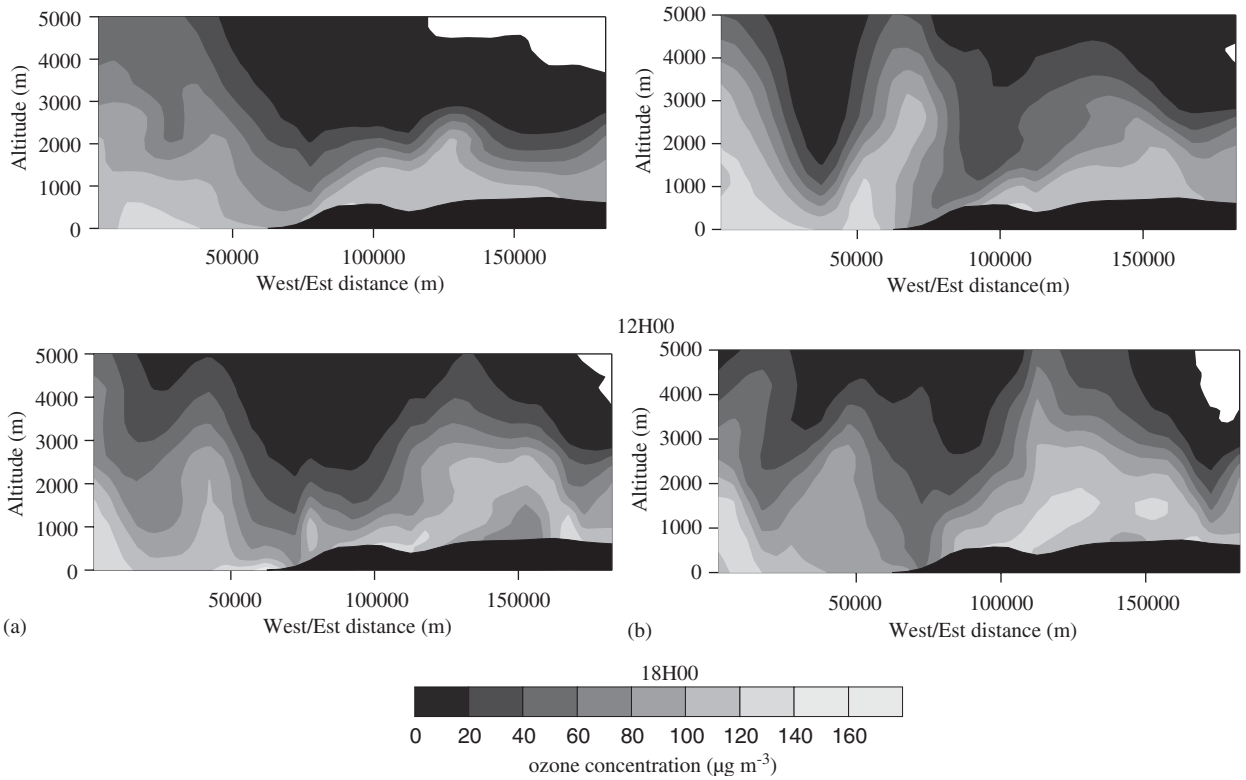

Fig. 6. Vertical O_3 concentrations fields at 12 and 18 UTC for (a) 15 June 2000 and (b) 16 June 2000.

The presented cross-sections are at latitude 40.11 °N, between 9.41 °W and 7.19 °W longitude (*XZ* plane over Estarreja station).

Major differences in O_3 concentration patterns are found at noon. The second day of simulation presents stronger oscillating curves in O_3 concentration and it is possible to observe higher values near coastline. At noon, the combined effects of O_3 boundary concentrations and updraft motions near the west domain's boundary explain the vertical O_3 distribution. At 18 UTC the O_3 concentration meanders are very pronounced, indicating the stronger vertical movements previously identified. As mentioned in Section 3.1, O_3 sensitivity analysis to land use and topography over the inner domain is performed according to the procedure developed by Stein and Alpert (1993). The analysed fields ($\hat{f}_i$ and $\hat{f}_{ij}$) are based on the equations proposed by the authors for two factors analysis. The O_3 concentrations fields obtained are labelled according to the four simulations described (see Table 1). Hence, fields are obtained for the control simulation (f_{12}), for the flat terrain simulation (f_2), for the constant land use category simulation (f_1) and for the simulations were these two factors are set also constant, i.e., flat terrain and constant land use category (f_0). To detect the contribution of these factors to the vertical O_3 distribution it is necessary to observe the fields defined by

$$\hat{f}_0 = f_0, \qquad \hat{f}_1 = f_1 - f_0,$$
$$\hat{f}_2 = f_2 - f_0, \quad \hat{f}_{12} = f_{12} - (f_1 + f_2) + f_0,$$

where $\hat{f}_0$ shows the O_3 concentration not related with either of the two factors under analysis; $\hat{f}_1$ shows the vertical O_3 concentration induced by the topography; $\hat{f}_2$ shows the influence of constant land use and finally, $\hat{f}_{12}$ gives information related to the interaction of these two factors on the vertical O_3 concentration field. Results of these estimated fields are presented in Figs. 7 and 8. It is possible to observe that vertical meanders are almost vanished for the simulation where flat terrain and constant land use are considered, although some O_3 spots appear below 5 km altitude. For these conditions higher O_3 concentrations are observed in higher altitudes over land. The analysis of Figs. 7 and 8 reveals that an enhancement of O_3 concentrations is verified especially over water, western part of the domain, being more pronounced when topography

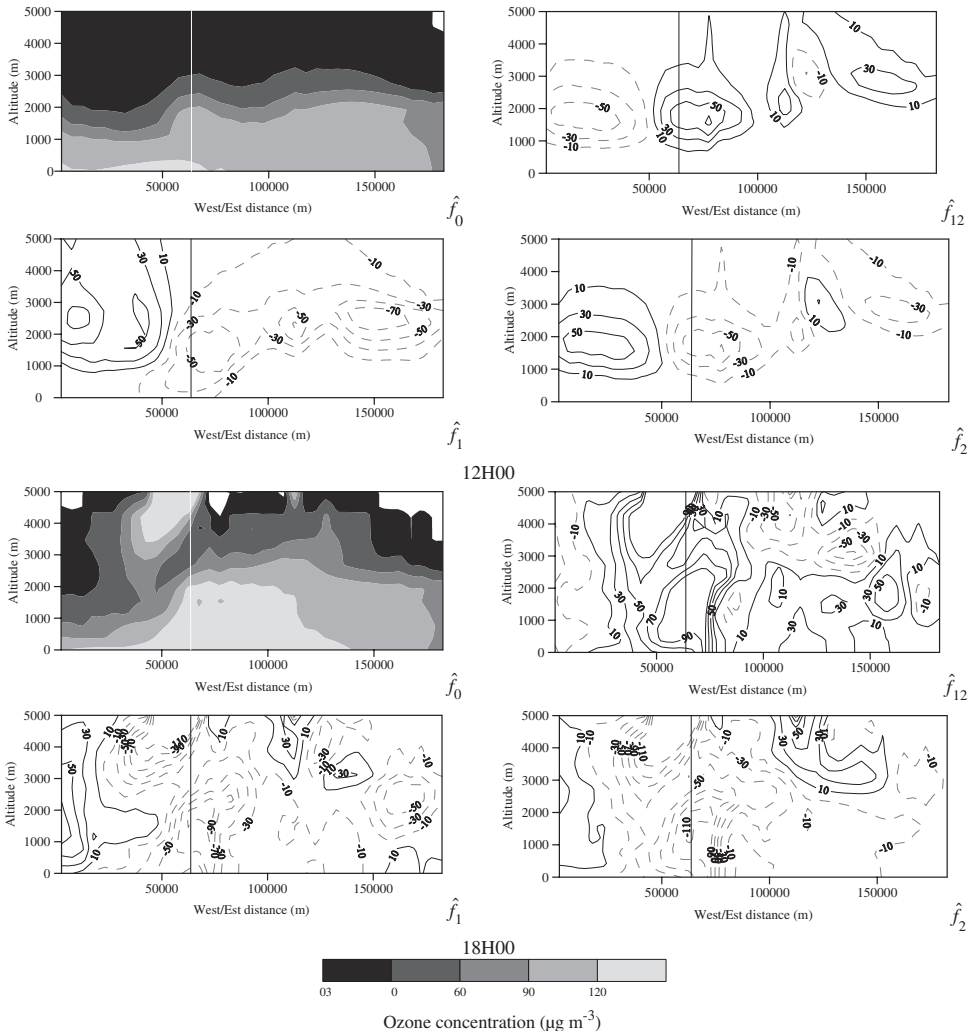

Fig. 7. O_3 concentrations unrelated to either topography and land use ($\hat{f}_0$); O_3 concentrations induced by topography ($\hat{f}_1$); O_3 concentrations induced by land use ($\hat{f}_2$); and O_3 concentration induced by the interaction between topography and land use ($\hat{f}_{12}$), for 15 June 2000 at 12 UTC and 18 UTC. Vertical line represents shore location.

is the inductor factor ($\hat{f}_1$). At noon, O_3 concentrations are highly promoted in the western part of the domain for both factors ($\hat{f}_1$ and $\hat{f}_2$) for the two simulated days, as well as its horizontal extension. This feature is also detected at 18 UTC but is less intense. On the other hand, land-use effects are more related with O_3 diminishing values over land (centre and east part of the domain).

The contour lines values reveal that topography represents a leading factor in O_3 transport to the higher levels in the western part of the domain. Increases in O_3 concentrations are visible at higher levels, reaching approximately $70\,\mu g\,m^{-3}$ at 3 km altitude and above (Fig. 8 at 12 UTC). The interaction between both factors promotes increases in O_3 concentrations above shore line reaching $90\,\mu g\,m^{-3}$ at 18 UTC in both days. At this time of the day, the vertical extent of these increases is higher, reaching 5 km altitude, which makes O_3 available in a residual layer. At 12 UTC the O_3 increases are also visible over land but a negative contribution is observed over water. In general, the O_3 concentrations increasing or decreasing amounts may depend on the weather situation imposed by the boundary conditions, although the O_3 patterns are maintained.

5. Concluding remarks

This work investigates the main flow patterns that govern the pollutants dispersion in the Atlantic

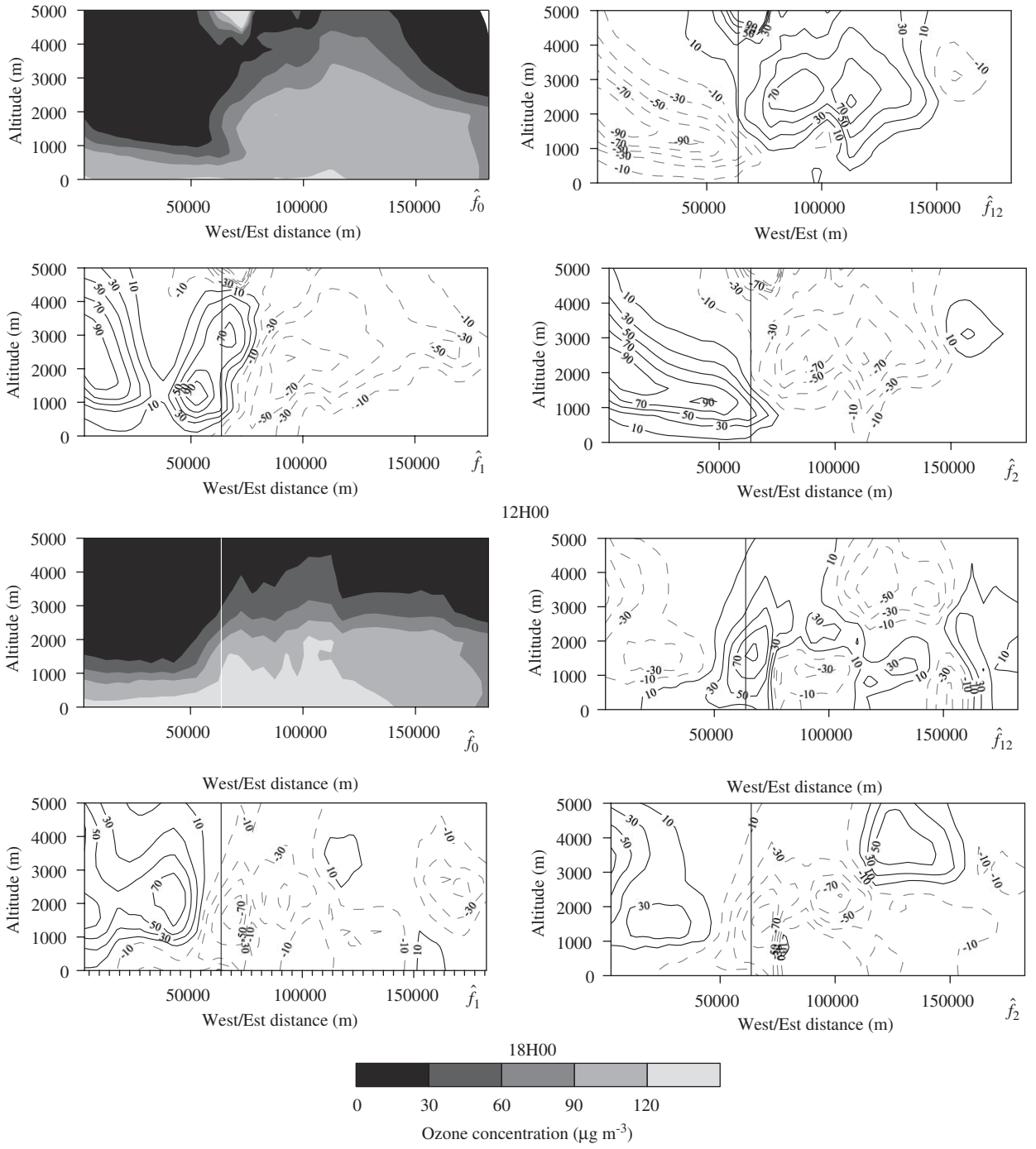

Fig. 8. O_3 concentrations unrelated to either topography and land use ($\hat{f}_0$); O_3 concentrations induced by topography ($\hat{f}_1$); O_3 concentrations induced by land use ($\hat{f}_2$); and O_3 concentration induced by the interaction between topography and land use ($\hat{f}_{12}$), for 16 June 2000 at 12 and 18 UTC. Vertical line represents shore location.

coast of the Iberian Peninsula. The MM5/MARS system of models is applied to northern part of Portugal during a two days O_3 episode. As a first attempt, a numerical interface between MM5 and MARS is built up. Validation procedures and sensitivity studies are carried on. The sensitivity

studies focus on the relative importance between water presence and topographic effects in vertical O_3 concentrations patterns.

The meteorological model validation indicates that the MM5 model reproduces quite well the daily-temperature evolution but wind speed and direction need more attention on model refinements in future applications. Both meteorological stations are near shore but MM5 reproduces better the daily-wind behaviour in the northern station. The MARS model follows the measured concentrations for the three air-quality stations, although it overestimates O_3 concentrations over night periods and underestimates O_3 peaks at industrial and rural sites. This work helps to identify some relevant points for future air-quality applications with a system of models that includes MM5. Concerning this model, a horizontal resolution greater than $5\,km \times 5\,km$ will be helpful for a better definition of the coast line benefiting meteorological simulation over regions semi-surrounded by water, as Aveiro region. On the other hand, meteorological data assimilation would help to simulate, in a more accurate manner, the north-western border of the Iberian Peninsula Thermal Low, where strong pressure gradients are verified. Concerning the photochemical model MARS, daily-emission functions for industrial sources, considering both point and diffuse classification, should be included, in order to better resolve nocturnal O_3 consumption. A major improvement would be the inclusion of different air-quality boundary conditions, on western and eastern domain's boundaries, during thermal low synoptic conditions based on air-quality campaigns data. The performed sensitivity studies allow to better understand the role of topography/water presence in mesoscale circulations and consequently on atmospheric-pollutants dispersion, namely on O_3 concentration patterns. As shown in other studies, the Iberian thermal low creates very intense vertical motion cells that are developed over the Peninsula. MM5 model clearly simulates this synoptic situation and allows the visualisation of more detailed isentropic vertical structure in the atmosphere. The presence of complex topography near the coast line is more effective on the intensification and complexity of vertical movements when compared with thermal gradient induced only by different physical characteristics between land/sea underlying surfaces, as shown in the isotach fields of the vertical wind component. The performed sensitivity analysis gives the indication that topography is the main driving force mechanism on air pollutants injection on higher tropospheric levels in the studied coastal region and for the simulated meteorological conditions.

Acknowledgements

The authors are grateful to the Portuguese Foundation for Science and Technology and the European Social Fund, for the Structural Funds period between 2000–2006, for the Ph.D. grants of A. C. Carvalho (PRAXIS XXI/BD/21474/99) and A. Carvalho (SFRH/BD/10882/2002). The authors also gratefully acknowledge the Portuguese Environment Regional Directorate Centre for the accessibility to the measured air-quality data and financial support by the Acción Integrada España-Portugal HP1999-0057 granted by the Portuguese Universities Rectors Board.

References

Alder, B., Fernbach, S., Rotenberg, M. (Eds.), 1977. Methods in Computational physics: Advances in Research and Applications, vol. 1–17. Academic Press, New York.

Baldasano, J.M., Costa, M., Cremades, L., Flassak, T., Wortmann-Vierthaler, M., 1993. Influence of traffic conditions on the air quality of Barcelona during the Olympic Games'92. In: Gryning, S.-E., Millán, M.M. (Eds.), Proceedings of the Air pollution Modelling and Its Application X. Plenum Press, New York, USA, pp. 643–644.

Barna, M., Lamb, B., 2000. Improving ozone modeling in regions of complex terrain using observational nudging in a prognostic meteorological model. Atmospheric Environment 34, 4889–4906.

Barros, N., 1999. Poluição atmosférica por foto-oxidantes: o ozono troposférico na região de Lisboa (Atmospheric pollution by photo-oxidants: tropospheric ozone over Lisbon region). Ph.D. Thesis, University of Aveiro, Portugal.

Barros, N., Borrego, C., Toll, I., Soriano, C., Jiménez, J., Baldasano, J.M., 2003. Urban photo-chemical pollution in the Iberian Peninsula: Lisbon and Barcelona Airsheds. Air & Waste Management 53, 347–359.

Borrego, C., Barros, N., Miranda, A.I., Carvalho, A.C., Valinhas, M.J., 1998. Validation of two photo-chemical numerical systems under complex mesoscale circulations. In: Gryning, S.-E., Batchvarova, E. (Eds.), Proceedings of the 23rd International Techical Meeting of NATO/CCMS on Air Pollution Modelling and its Application. Plenum Press, New York, USA, pp. 597–604.

Borrego, O., Tchepel, O., Barros, N., Miranda, A.I., 2000. Impact of road traffic emissions on air quality of the Lisbon region. Atmospheric Environment 34, 4683–4690.

Choi, H., 2003. Increase of ozone concentration in an inland basin during the period of nocturnal thermal high. Water, Air and Soil Pollution: Focus 3 (5–6), 33–54.

Costa, M., 1995. Desenvolupament d'un model d'emissions atmosfèriques. Aplicació a l'Àrea Geogràfica de Barcelona (Development of an atmospheric emissions model. Aplication

to Barcelona geographic area). Ph.D. Thesis, Universitat Politècnica de Catalunya, Spain.

Dudhia, J., 1993. A nonhydrostatic version of the Penn State—NCAR mesoscale model: Validation tests and simulation of an Atlantic cyclone and cold front. Monthly Weather Review 121, 1493–1513.

Elbern, H., Schmidt, H., 2001. Ozone episode analysis by four-dimensional variational chemistry data assimilation. Journal of Geophysical Research 106, 3569–3590.

European Commission (EC), 1994. Corinair technical annexes: default emission factors handbook, vol. 2. Office for Official Publications of the European Communities, Brussels.

Ferreira, J., Carvalho, A., Carvalho, A.C., Monteiro, A., Martins, H., Miranda, A.I., Borrego, C., 2003. Chemical Mechanisms in two photo-chemical modelling systems: a comparison procedure. In: Borrego, C., Incecik, S. (Eds.), Proceedings of the Air Pollution Modelling and its Application XVI. Kluwer Academic/ Plenum Publishers, New York, USA, pp. 87–96.

Grell, G., Dudhia, J., Stauffer, D., 1994. A description of fifth-generation Penn State/NCAR mesoscale model (MM5), NCAR Tech. Note NCAR/TN-398 + STR, Boulder, p. 122.

Hoinka, K.P., Castro, M., 2003. The Iberian Peninsula thermal low. Quarterly Journal of the Royal Meteorological Society 129, 1491–1511.

Keyser, D., Anthes, R.A., 1977. The applicability of a mixed-layer model of the planetary boundary layer to real-data forecasting. Monthly Weather Review 105, 1351–1371.

Martín, F., Palacios, M., Crespi, S., 2001. Simulations of mesoscale circulations in the center of the Iberian Peninsula for thermal low pressure conditions. Part I: Evaluation of the topography vorticity-mode mesoscale model. Journal of Applied Meteorology 40, 880–904.

Millan, M., Artiñano, B., Alonso, L., Castro, M., Fernandez-Patier, R., Goberna, J., 1992. Mesometeorological Cycles of air pollution in the Iberian Peninsula. Air Pollution Research Report 44, European Community Commission, Brussels.

Millán, M., Salvador, R., Mantilla, E., Artiñano, B., 1996. Meteorology and photo-chemical air pollution in Southern Europe: experimental results from EC research projects. Atmospheric Environment 30, 1909–1924.

Millán, M.M., Salvador, R., Mantilla, E., Kallos., G., 1997. Photo-oxidant dynamics in the western mediterranean in summer: results from european research projects. Journal of Geophysical Research 102 (D7), 8811–8823.

Miranda, A.I., Martins, H., Monteiro, A., Ferreira, J., Carvalho, A.C., Borrego, C., 2002. Evaluation of two mesoscale modeling systems using different chemical mechanisms. In: American Meteorological Society (Eds.), Proceedings of the Fourth Symposium on the Urban Environment, Joint Session. Boston, USA, pp. J77–J78.

Monteiro, A., 2003. Poluição atmosférica na região de Aveiro: modelação de mesoscala e sua validação (Atmospheric pollution in Aveiro region: mesoscale simulation and its validation). M.Sc. Thesis, University of Aveiro, Portugal.

Monteiro, A., Vautard, R., Borrego, C., Miranda, A.I., 2005. Long-term simulations of photo-oxidant pollution over Portugal using the CHIMERE model. Atmospheric Environment 39, 3089–3101.

Moussiopoulos, N., Sahm, P., Kessler, C., 1995. Numerical simulation of photo-chemical smog formation in Athens, Greece a case study. Atmospheric Environment 29, 3619–3632.

Pielke, R.A., 2002. Mesoscale Meteorological Modeling. Academic Press, San Diego, CA.

Salvador, R., Millán, M.M., Mantilla, E., Baldasano, J.M., 1997. Mesoscale modelling of atmospheric processes over the western Mediterranean area during summer. International Journal of Environmental Pollution 8, 513–529.

San José, R., Pietro, J.F., Martín, J., Delgado, L., Jimenez, E., González, R.M., 1997. Integrated environmental monitoring, forecast and warning systems in metropolitan areas (EMMA): Madrid application. In: San José, R., Brebbia, C.A. (Eds.), Proceedings of the First International Conference on Measurements and Modelling in Environmental Pollution. Computational Mechanics Publications. Southampton, England, pp. 313–323.

Seaman, N.L., 2000. Meteorological modeling for air-quality assessments. Atmospheric Environment 34, 2231–2259.

Schneider, C., 1994. Emissionskataster zur berechnung der ausbreitung von luftschadstoffen. Verlag, Duesseldorf.

Sistla, G., Winston, H., Jia-Yeong, K., Kallos, G., Zhang, K., Mao, H., Rao, S.T., 2000. An operational evaluation of two regional-scale ozone air-quality modeling systems over the Eastern United States. Bulletin of the American Meteorological Society 82, 945–964.

Stein, U., Alpert, P., 1993. Factor separation in numerical simulations. Journal of the Atmospheric Sciences 50 (14), 2107–2115.

Stull, R.B., 1991. An Introduction to Boundary Layer Meteorology. Kluwer Academic Publishers, Dortrecht, The Netherlands.